Molecular Crystals and Liquid Crystals
Publication details, including instructions for authors and subscription information:
http://www.tandfonline.com/loi/gmcl16

Nonlinear Optical Effects in the Nematic Phase

D. Armitage [a] & S. M. Delwart [a]
[a] Lockheed Palo Alto Research Laboratory, Palo Alto, California, 94304
Version of record first published: 17 Oct 2011.

To cite this article: D. Armitage & S. M. Delwart (1985): Nonlinear Optical Effects in the Nematic Phase, Molecular Crystals and Liquid Crystals, 122:1, 59-75

To link to this article: http://dx.doi.org/10.1080/00268948508074742

Mol. Cryst. Liq. Cryst., 1985, Vol. 122, pp. 59–75
0026-8941/85/1224–0059/$20.00/0

Nonlinear Optical Effects in the Nematic Phase

D. ARMITAGE and S. M. DELWART

Lockheed Palo Alto Research Laboratory, Palo Alto, California 94304

(*Received July 30, 1984*)

Large nonlinear optical effects are associated with nematic order. This is due to reorientation of the nematic by the optic field and or reduction in nematic order by absorption of optical energy. These effects were analyzed taking into account viscosity and turbidity. Experiments were performed using an absorption cell containing dye doped pentylcyanobiphenyl. A thermal grating is induced by absorbing interfering 10-ns YAG laser pulses. The grating is continuously monitored by a HeNe laser readout. The amplitude and response time of the grating increase as the isotropic phase transition temperature is approached. A diffraction efficiency of 1 percent with 200-ns response is observed for a write energy of 1 mJ/cm^2, 1°C below the transition temperature. Modulating the thermal grating across the phase transition produces an index grating with a nonthermal decay characteristic $\sim$10 ms, typical of the reorientation time of a disordered nematic.

INTRODUCTION

Nonlinear optics is concerned with effects such as harmonic generation and wave mixing which follow from a nonlinear dependence of polarization on electric field.[1] The response at optical frequencies in the liquid crystal phase is discussed elsewhere.[2] Here we are interested in nonlinearities based on director reorientation and thermal effects in the nematic phase.

The control of director orientation by a static magnetic or electric field has been established for many years. It follows as a direct consequence that the director will be influenced by an optical field. This has been demonstrated in recent years; however, the effect was observed much earlier.[3–10] The current activity stems from potential application of liquid crystals in nonlinear optical devices.

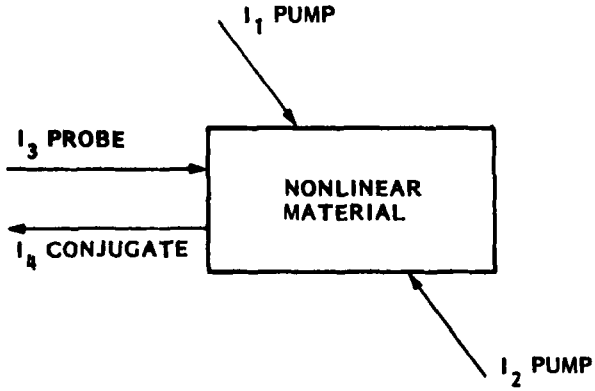

FIGURE 1 Degenerate four-wave mixing.

For example, the phase conjugate operation is of particular interest in optical systems.[11, 12] In identifying the wavefront phase distribution $\phi(x, y)$, a phase conjugate operation produces a counterpropagating wave with opposite phase $-\phi(x, y)$. Therefore, it is possible to construct systems where the phase aberrations are automatically cancelled by a double pass through the distorting media via a phase conjugate mirror.

Figure 1 shows phase conjugation via degenerate four-wave mixing. This can be interpreted as the interaction of the probe and pump beams to form a hologram in the nonlinear medium, which is also read by the pump beam. The relation between the four waves is described analytically in terms of the nonlinear third-order susceptibility tensor. The advantage of liquid crystals in such applications is a very large effect for small input power. The disadvantage is a slow viscous response and optical path length limited by turbidity.

The response can be accelerated by increased optical power. Eventually the retarding force is dominated by viscosity. We calculate the response in this regime.

Recently it has been observed that the thermal grating response of a nematic is unusually large.[13-15] The property exploited is the temperature dependence of the refractive index. This effect has considerable history, where prior experiments used a solvent containing a dye, e.g., rhodamine 6G in ethanol.[16, 17] The optical energy is absorbed by the dye and then transferred to the solvent, resulting in a thermal grating and consequent index grating. The time constant of this process in ordinary liquids is of nanosecond order.

The temperature sensitivity of the nematic refractive index, particu-

larly close to the isotropic phase transition, is determined by the temperature dependence of the order parameter. However, the greater sensitivity is associated with a larger response time of 100-ns order. We show that when submillisecond response is demanded, the thermal effect is more efficient than the orientation effect.

TURBIDITY

Turbidity is a distinctive feature of the nematic phase. This is a consequence of large birefringence and weak elasticity. These properties favor low power devices. The optical path length in a nematic device is limited $\sim 100\ \mu m$ by turbidity. The following expression for the optical scattering cross section can be written in the limit $\Delta n/n \to 0$[18]

$$\sigma = V(\epsilon_a \pi/\lambda^2)^2 (kT/Kq^2)P$$

where σ = scattering cross section/solid angle, V = volume = Ad, ϵ_a = optical dielectric anisotropy = $2n\Delta n$, λ = vacuum wavelength $= 5 \times 10^{-5}$ cm, kT = thermal energy, K = elastic constant $\simeq 10^{-6}$ dyne, q = scattering vector = $(4\pi n \sin 1/2\phi)/\lambda$, ϕ = scattering angle, n = refractive index = 1.5, Δn = birefringence = 0.2, P = polarization and orientation factor $\simeq 1$; for the case shown in Fig. 2, we calculate $P = 1.5$.

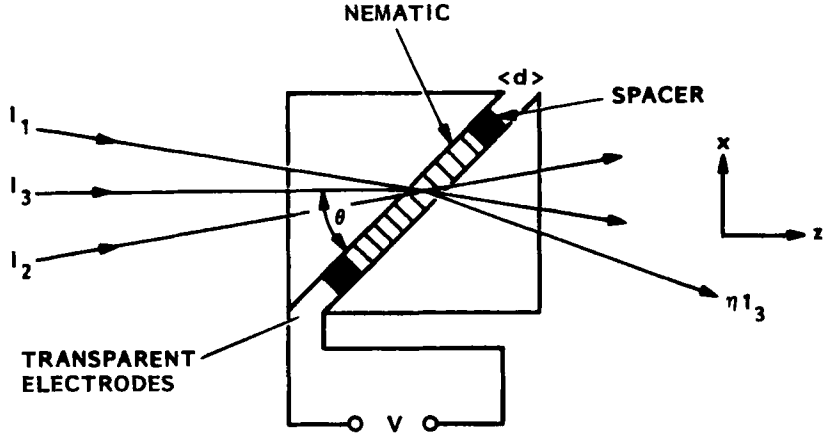

FIGURE 2 Configuration of liquid crystal, laser beams, and electric fields.

The integrated scattering is written

$$2\pi \int_{\phi_0}^{\pi} \sigma \sin\phi \, d\phi = 1.6 \times 10^{-4}\ \mathrm{K}^{-1} \Delta n^2 A d \ln(2/\phi_0) \tag{2}$$

where ϕ is a minimum angle determined by the minimum energy of fluctuations. The nematic is contained in an optical cell with spacing $d < 200\ \mu$m. Assuming a strong anchoring condition, the minimum distortion energy corresponds to taking $q = \pi/d$ or $\phi_0 = \lambda/2\mathrm{nd} = 3.4 \times 10^{-3}$.

Hence, the scattering attenuation of optical intensity I is written

$$I \propto \exp(-ad) = \exp(1.6 \times 10^{-3}\ \mathrm{K}^{-1} \Delta n^2 d) \tag{3}$$

The result is insensitive to the choice of ϕ_0. For typical values, the $1/e$ point $\simeq 0.2$ mm.

ORIENTATIONAL RESPONSE

A beam propagating at θ to the nematic axis as shown in Fig. 2 experiences a local birefringence $\Delta n \sin^2\theta$, in the limit $\Delta n \ll n$. This exerts a torque given by[7]

$$\text{Torque} = 2I\Delta n c^{-1} \sin\theta \cos\theta \tag{4}$$

where $c = 3 \times 10^{10}$ cm/s and $\theta = 45°$ for maximum torque.

Coherent input beams, as shown in Fig. 2, give an intensity distribution in the nematic.

$$I = I_1 + I_2 + 2(I_1 I_2)^{1/2} \cos qx \tag{5}$$

This modulates the nematic orientation at spatial frequency $\Lambda = 2\pi/q$, producing a phase grating. Using the thin phase grating approximation ($J_1^2(\psi) = \psi^2/4$), the equilibrium diffraction efficiency has the form.[7]

$$\eta_0 = I_1 I_2 \left[\frac{\Delta n^2 d}{\lambda c K (4\Lambda^{-2} + d^{-2})} \right]^2 \tag{6}$$

substituting typical values gives $\eta_0 \simeq 1$ percent for $(I_1 I_2)^{1/2} \simeq 1$ W/cm^2, when $d = \Lambda = 100\ \mu$m.

In the high speed limit the response is viscous limited. Therefore, ignoring the elasticity gives the torque balance equation.

$$I\Delta n/c = \gamma\, d\theta/dt \tag{7}$$

where γ = effective viscosity $\sim$0.1 poise.

This implies a diffraction efficiency[19]

$$\eta_0 = I_1 I_2 (2\pi d \Delta n^2 \Delta t \gamma^{-1} \lambda^{-1} c^{-1})^2 \tag{8}$$

where Δt is the integration time.

Taking into account turbidity, I should be averaged according to $\exp(-\alpha z)$ and η_0 attenuated $\exp(-\alpha d)$. Hence, Eq. (8) becomes

$$\eta = \eta_0 (\alpha d)^{-2} [1 - \exp(-\alpha d)]^2 [\exp(-\alpha d)] \tag{9}$$

substituting Eqs. (3) and (8) gives a maximum

$$\max \eta = 2 \times 10^6 I_1 I_2 (\Delta t\, \mathrm{K} \gamma^{-1} \lambda^{-1} c^{-1})^2 \tag{10}$$

when

$$\exp(1.6 \times 10^{-3}\, \mathrm{K}^{-1} \Delta n^2 d) = 3 \tag{11}$$

If d is optimized according to Eq. (11), η favors materials with high $(K/\gamma)^2$. Substituting the given typical values and requiring $\eta = 1$ percent for $\Delta t = 10^{-3}$ s gives $(I_1 I_2)^{1/2} = 1000$ W/cm^2 and optimum $d = 160$ μm.

Equation (6) can be similarly optimized for turbidity. Making the assumption $\Lambda < d$, optimum $d \simeq 160$ μm and $\eta \simeq 0.1$ η_0. However, the averaging process used in deriving Eq. (9) introduces error in this case. The η described here characterizes the performance in a 4-wave mixing configuration.

SUPPRESSION OF SCATTERING BY APPLIED ELECTRIC FIELD

Applying an electric field reduces the thermal fluctuations and hence light scattering.[18,20] Therefore, η could be raised by increasing d.[19]

The applied electric field introduces an energy term $E^2 \Delta\epsilon/2$, where $\Delta\epsilon$ is the low-frequency permittivity anisotropy. This term is added to

the elastic term Kq^2, and the scattering cross section becomes[18, 20]

$$\sigma_E = \sigma_0 Kq^2/(Kq^2 + E^2\Delta\epsilon/2) \tag{12}$$

Integrating as before, results in a field-dependent beam attenuation

$$I = \exp\left[-7.84 \times 10^{-5}\Delta n^2\,\mathrm{K}^{-1}\ln(1 + 2.8 \times 10^{11}K/E^2\Delta\epsilon)\right] \tag{13}$$

Taking an upper limit $E = 10^5$ V/cm and $\Delta\epsilon = 10\epsilon_0$, the $1/e$ point becomes 2.2 mm, which is a factor 15 over the zero field case.

The applied field also suppresses the optically written phase grating. However, since we are committed to short optical pulses, we can take advantage of the slow viscous relaxation when the applied field is removed.

When the field is switched off, the fluctuations grow at rate

$$\tau = \gamma/Kq^2 \tag{14}$$

for

$$\tau\langle\Delta t, q^2\rangle\gamma/K\Delta t \tag{15}$$

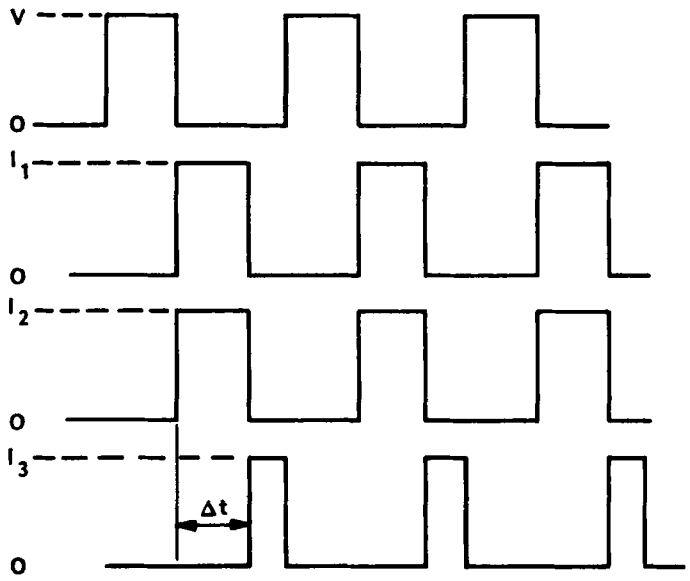

FIGURE 3 Sequence of laser and voltage pulses.

This implies a higher cutoff angle ϕ_0 in the scattering integral. Approximating ϕ_0 according to $q^2 = \gamma/K\Delta t$, the beam attenuation becomes

$$I = \exp\{-79\Delta n^2 d[26 + \ln(K\Delta t/\gamma)]\}$$

for $\Delta t = 10^{-3}$ s the $1/e$ point is 0.44 mm, which is 2.9 over the zero field case, implying $\eta \times (2.9)^2$. Figure 3 indicates the pulse sequence.

THERMAL GRATINGS

The absorption of optical energy is associated with a temperature rise and hence a change in refractive index. This effect is exploited in the dye cell, where the absorption is controlled by a dye which is solubilized in a solvent chosen for high dn/dT.[16, 17, 21, 22]

In the nematic phase, dn/dT is exceptionally large. A wide range of soluble dyes are available. The potential of thermal gratings in nematics has already been recognized.[13] We analyze the performance of the nematic dye cell as follows.

Assume intersecting laser beams of equal intensity I, which give an interference pattern

$$\text{intensity} = 2I(1 + \sin qx) \tag{16}$$

The absorbed energy spatially modulates the refractive index, which in the adiabatic approximation is written

$$\delta n = 2C^{-1} dn/dT\, It\alpha \exp(-\alpha z)\sin qx \tag{17}$$

In the thin phase approximation ($J_1^2(\psi) = \psi^2/4$)

$$\eta = (2\pi/\lambda)^2 I^2 t^2 C^{-2}(dn/dT)^2[1 - \exp(-\alpha d)]^2 \exp(-\alpha d) \tag{18}$$

where t = integration time, C = heat capacity/volume, T = temperature, α = absorption coefficient.

This is maximum at $\alpha = 1.1/d$ when

$$\eta = 5.85 I^2 t^2 \lambda^{-2} C^{-2}(dn/dT)^2 \tag{19}$$

Clearly, the material property $C^{-2}(dn/dT)^2$ should be maximized.

The refractive index can be approximated.[23]

$$dn_e/dT = 1/2n_i\, d\rho/dT + 2/3\Delta n'\, dS/dT \tag{20}$$

$$dn_0/dT = 1/2n_i\, d\rho/dT - 1/3\Delta n'\, dS/dT \tag{21}$$

where n_e = extraordinary index, n_0 = ordinary index, n_i = index in isotropic phase, ρ = density, S = order parameter, $\Delta n' = \Delta n/S$.

Clearly $|dn_e/dT| > |dn_0/dT|$. As the isotropic point is approached, dS/dT dominates and $|dn_e/dT| \to |2dn_0/dT|$. The normalized birefringence $\Delta n/S$ should be used in comparing nematogens.

The mean field approximation[23]

$$S = \left(1 - 0.98TV^2/T_nV_n^2\right)^{0.22} \tag{22}$$

gives some indication of the behavior over a wide temperature range.

Experimental data for methoxybenzylidenebutyaniline (MBBA) and pentylcyanobiphenyl (5CB) are available. Two sets of refractive index data were compared for each material and found consistent when expressed in terms of reduced temperature $T_n - T$.[24-26] The heat capacity as a function of temperature is available for MBBA.[27,28] For 5CB the value at $T_n - T = 10°K$ is known,[29] and assuming the same reduced temperature dependence as MBBA should introduce negligible error in this calculation.

The experimental values of $C^{-2}(dn/dT)^2$ are plotted against reduced temperature in Fig. 4. The values derived from the mean field expression (22) are also plotted. As expected, the mean field approximation is poor close to the transition point.

There is about a factor 100 variation with temperature. At $T_n - T = 1°K$, the predicted 5CB, $\eta = 1$ percent for input energy 0.8 mJ/cm^2.

A further advantage of the nematic follows from the incorporation of pleochroic dyes.[30] The dye is oriented by the nematic and results in a polarization-dependent absorption coefficient. This can be exploited by orthogonally polarized write and read beams. The ratio of optical densities can be written.[30]

$$L \text{ dye } \alpha_e/\alpha_0 = r_L = (1 + 2S)/(1 - S) \tag{23}$$

$$T \text{ dye } \alpha_0/\alpha_e = r_T = (2 + S)/(1 - S) \tag{24}$$

where L and T refer to dyes absorbing light polarized along or

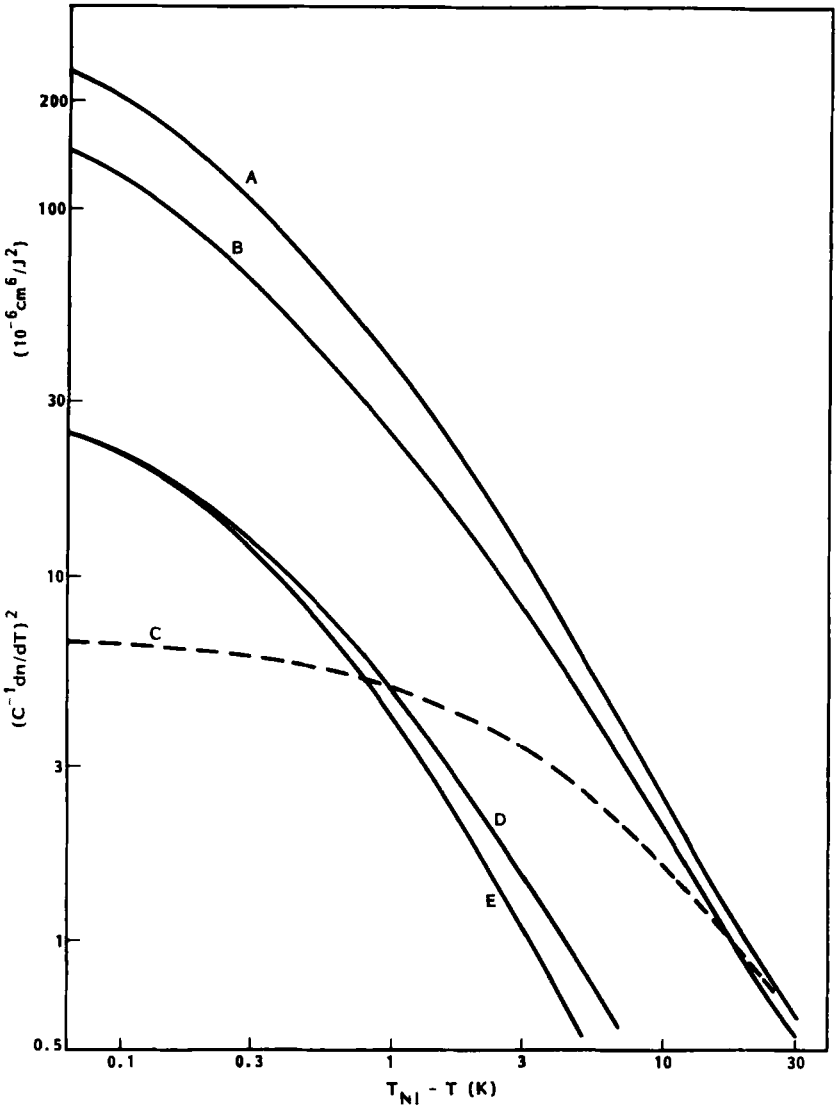

FIGURE 4 Nematic materials parameter $(C^{-1}\, dn/dT)^2$ against reduced temperature $T_n - T$. (A) MBBA extraordinary axis, (B) 5CB extraordinary axis, (C) mean-field prediction for 5CB extraordinary axis, (D) MBBA ordinary axis, (E) 5CB ordinary axis.

perpendicular to the optic axis. The order parameter of the dye in the liquid is approximately the same as the nematic order parameter.

Substituting the α ratios in Eq. (18) and recalculating the maximum gives the result

$$\eta_L = 39.5\left[1 - (1 + 2r_L)^{-1}\right]^2 (1 + 2r_L)^{-1/r_L} I^2 t^2 \lambda^{-2} C^{-2} (dn_0/dT)^2 \tag{25}$$

$$\eta_T = 39.5\left[1 - (1 + 2r_T)^{-1}\right]^2 (1 + 2r_T)^{-1/r_T} I^2 t^2 \lambda^{-2} C^{-2} (dn_e/dT)^2 \tag{26}$$

Note the association of L with n_0 and T with n_e. The dyes are more effective for increasing S, but high dS/dT favors low S. Substituting $S = 0.5$ in Eqs. (23)–(26) gives $\eta_L = 3.08\ \eta_0 I$ and $\eta_T = 2.29\ \eta_{eI}$, where η_I = the efficiency for a polarization independent dye. This is about the level of improvement that can be attained in pursuit of high η, which is dominated by dS/dT hence $S < 0.5$.

In some applications, low attentuation of the readout beam is important. Therefore, expanding the exponentials in Eq. (18)

$$\alpha d \ll 1, \qquad \eta_T = r_T^2 \eta_{eI} \tag{27}$$

with a similar expression for η_L. It should be noted that for $T_n - T > 20°\text{K}$, $r_T^2 > 10$ and $r_L^2 > 30$

EXPERIMENTAL

The nematogen used in the experiments was 5CB containing a small quantity of L-dye D81 (EM Chemicals). The glass sample cell spacing was 10 or 100 μm, (Hellma Cells). Uniform parallel alignment of the nematic was achieved by the rubbed PVA process. The glass sample cell was inserted into a temperature controlled aluminum block.

Figure 5 shows the optical arrangement. A 10-μm period thermal grating is written via M1 and M2. Continuous readout with a HeNe laser records the grating evolution. Insertion of M3 allows readout with the YAG pulse.

Pure 5CB, without dye, fails to show diffraction for write energy as high as 0.2 J/cm^2. Inclusion of a small quantity of dye provides optical absorption, and diffraction is easily seen.

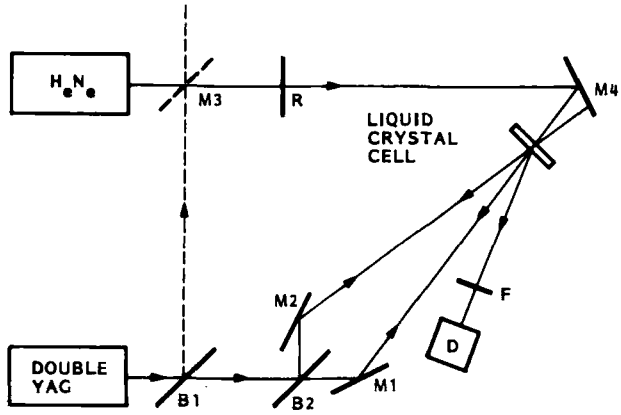

FIGURE 5 Optical arrangement, M1, M2, M3, M4 mirrors, B1, B2 beamsplitter, R polarization control, F red filter, D diode detector.

The first-order diffraction intensity is recorded on a storage oscilloscope. The YAG pulse is 10 ns long, and the detector time constant is 10 ns. This must be kept in mind when interpreting the scope trace.

The response time of the nematic to an absorbed energy pulse is determined by the order parameter response. Here a connection can be made to experiments on ultrasonic propagation.[31,32] The order parameter cannot change faster than a molecular vibration period. Since S is determined by the interactions of many molecules, the characteristic time is much longer than the molecular time scale. Moreover, as the phase transition point is approached, there is a slowing of order parameter response typical of critical phenomena.[18] This has been verified by ultrasonic experiments. Therefore, the thermal grating response time should be comparable with the ultrasonic data.[31,32]

Figure 6 shows the time evolution of the first-order diffraction intensity in the isotropic phase. An experimental time constant $\tau \simeq 30$ ns is indicated at $T - T_n = 6°K$. The time constant is not sensitive to temperature $T - T_n$. The magnitude of the time constant is comparable with ultrasonic result, $\tau = 25$ ns.[32] However in the ultrasonic case there is a strong temperature dependence $\tau \propto (T_n^* - T)^{-1}$.

Figure 7 shows similar recordings for the nematic phase at three temperatures. The time constant $\tau = 60$, 140, and 220 ns at $T_n - T = 14$, 2, and 0.4°K. The magnitude is of the same order, but greater than observed in the ultrasonic experiment. However, the temperature dependence is weaker.[32]

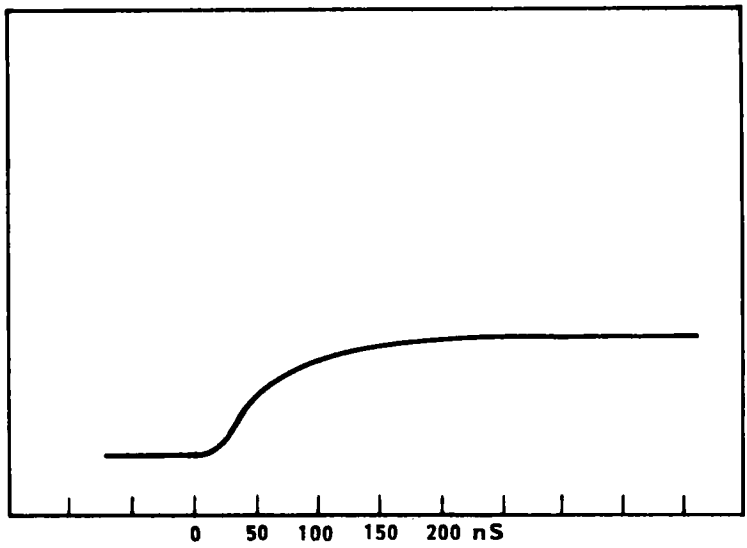

FIGURE 6 Time response of first-order diffraction intensity in isotropic phase of 5CB. $T - T_n = 6°K$. Cell thickness = 100 μm.

The decay of the thermal grating is determined by normal heat transfer processes. It can be shown[33] that the decay rate $\tau_d = (D_q^2)^{-1}$, where $D_e = 1.25 \times 10^{-3}$ and $D_0 = 7.9 \times 10^{-4}$ cm^2 s^{-1} in the extraordinary and ordinary directions respectively, and q is the grating wave vector. This is consistent with the decay trace shown in Fig. 8 for a 10-μm grating period.

The grating can be modulated into the isotropic phase, forming alternating layers of nematic and isotropic liquid. The discontinuity in

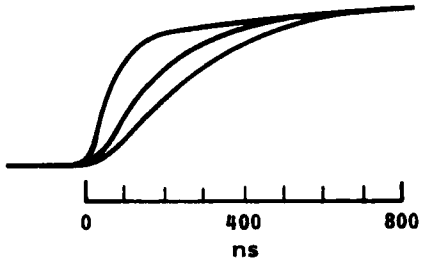

FIGURE 7 Rise time of first-order diffraction intensity in nematic phase of 5CB at $T_n - T = 14$, 2, and 0.4°K. Rise time increases at T approaches T_n. Cell thickness = 100 μm.

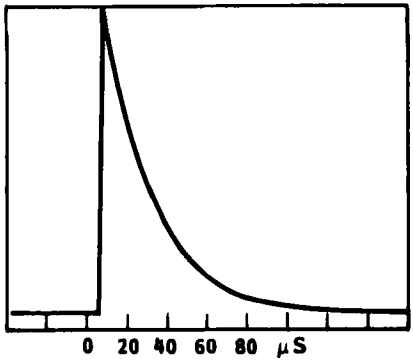

FIGURE 8 Decay of first-order diffraction intensity in nematic phase of 5CB at $T - T_n = 6°K$. Cell thickness = 100 μm.

refractive index ~0.1 at the nematic-isotropic interface implies a large amplitude, approximately rectangular phase grating. In this case 8 diffraction orders are visible. The rise time ~100 ns is consistent with Fig. 7.

The decay time as shown in Figs. 9 and 10 is of order 10 ms. This is much longer than the thermal decay. When modulated into the

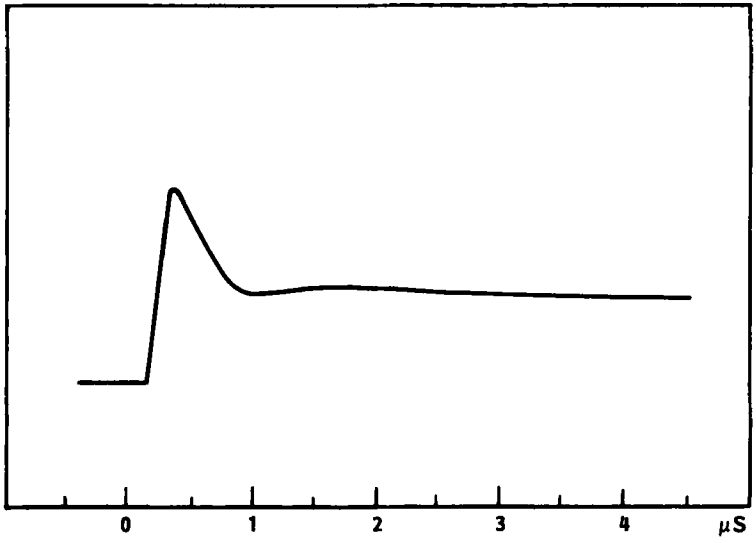

FIGURE 9 First-order diffraction intensity for modulation across nematic-isotropic transition cell thickness = 10 μm.

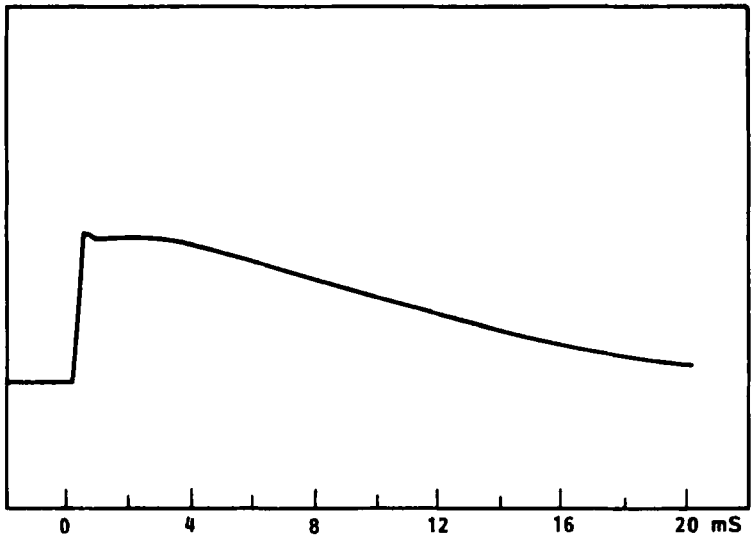

FIGURE 10 Decay of first-order diffraction intensity for modulation across nematic-isotropic transition. Cell thickness = 10 μm.

isotropic phase, the consequent rapid quench results in a disoriented nematic. The following reorientation of the nematic is viscous limited, which is consistent with a 10-ms time constant.

An initial peak or oscillatory response is shown in Fig. 9 and 10. The detail varies considerably from pulse to pulse. In this regime, a sinusoidal form is a poor approximation to the grating structure. Also, the transition to the isotropic is associated with large phase modulations $> 2\pi$. Therefore, the behavior should be sensitive to write pulse conditions. Detailed interpretation of these effects requires an improvement in experimental control.

The visibility of high-order diffractions is enhanced by the long integration time $\sim$10 ms. Readout with the YAG pulse restricts visibility to second-order.

The measured diffraction efficiencies η_e or η_0 as a function of temperature for $T_n - T > 1°C$ are consistent with data presented in Fig. 4. Discrepancies as large as a factor 2 can be attributed to fluctuations in the YAG output. For $T_n - T < 1°C$, the observed η does not achieve the predicted increase. This is explained by a number of practical restrictions. Fluctuations in the write pulse energy and hence average heating limit the temperature uniformity and stability. The light scattering increases close to the transition.

Acoustic waves can be generated by optical pulses. Laser induced phonon spectroscopy is a technique applied to the study of molecular processes.[34] In our case the 10-μm grating implies an acoustic period less than the 10-ns YAG pulse; therefore, the acoustic response is weak and can be neglected.

RESPONSE TIME

For an energy pulse input the order parameter response can be approximated

$$S = S_0 + \Delta S \exp(-t/\tau) \tag{28}$$

where S_0 is the new equilibrium value for the increase in energy or temperature. A single relaxation time τ is less applicable close to the transition point. The change in order ΔS controls the diffraction efficiency via Eq. (18):

$$\eta \alpha (dn/dT)^2 \alpha (\Delta S)^2 [1 - \exp(t/\tau)]^2 \tag{29}$$

The analysis of ultrasonic data is complicated by coupling to both the magnitude and local orientation of the order parameter.[31,32] There does not appear to be a simple connection between the optical and ultrasonic relaxation times.

In the isotropic phase the ultrasonic wave couples to scalar order parameter fluctuations.[18] An analytic treatment is consistent with experimental results.[32]

The order parameter fluctuations in the isotropic phase are a weak optical effect which is not directly significant in the thermal grating diffraction. Therefore, again there is no direct relation between the optical and ultrasonic relaxation. In the isotropic phase the refractive index change is due to density change $\Delta\rho$; therefore $\eta \alpha \Delta\rho^2$. Nematic correlation in the isotropic phase will influence the relaxation time observed in the optical experiment. However the weak temperature dependence of τ implies that this is not substantial.

The optical energy absorbed by the dye is transferred to the liquid crystal over a finite time known as the thermalization time. For ordinary solvents this is typically ~nanosecond, but can be as high as ~10 ns.[21,22] The observed response time in the isotropic phase could be attributed to dye thermalization and viscous limited response.

The order parameter response is now the difference between the nematic and isotropic phase responses. Because of the square law response in Eq. (29), the optical response should be about a factor 2 longer than the ultrasonic relaxation time. When these adjustments are made, $1/2(\tau - 30/2$ ns), becomes 22, 62, and 102 ns at $T_n - T = 14$, 2, and 0.4°K. This approaches the ultrasonic data, e.g., 16 and 50 ns at 14 and 2°K.[32]

CONCLUSION

We have derived a simple expression for the diffraction efficiency of the orientational response in the limit of viscous retarding force. This allows a simple incorporation of optical scattering effects to predict an optimum cell thickness $\sim$100 μm. A similar optimum follows when the elastic forces are included.

The thermal grating response of a nematic is analyzed. The large effects are related to the temperature dependence of the order parameter. The magnitude of the response is offset by an increasing response time as the transition temperature to the isotropic is approached.

The observed optical response time is related to ultrasonic relaxation rates. It is noted that the optical response time can be identified with the order parameter, allowing simple interpretation of the result.

At the nematic-isotropic transition, the response time $\sim$300 ns. Modulating the thermal grating into the isotropic phase results in a viscous limited decay associated with a quenched disordered nematic phase. These results could be of interest in the analysis of thermally written smectic display devices, where the picture element is pulsed into the isotropic phase.[29]

Acknowledgements

Discussion with G. Eyring, M. D. Fayer, H. J. Hoffman, and T. J. Karr and assistance from M. J. Murphy and R. E. Stone are acknowledged. The work is funded by the Lockheed Independent Research program.

References

1. A. Yariv, *Quantum Electronics*, (Wiley, 1975).
2. M. I. Barnik, L. M. Blinov, A. M. Dorozhkin, and N. M. Shtykov, *Mol. Cryst. Liq. Cryst.* V, 1–12 (1983).

3. R. M. Herman and R. J. Serinko, *Phys. Rev.* **A19** 1757–69 (1979).
4. I. C. Khoo, *Phys. Rev.* **A25**, 1636–1644, and **A26**, 1131 (1982).
5. B. Ya. Zel' Dovich and N. V. Tabiryan, *Zh. Eksp. Teor. Fiz.* **82**, 1126–1146 (1982) [*Sov. Phys. JETP* **55**, 656–666 (1982)].
6. S. M. Arakelyan, A. S. Karayan, and Yu. S. Chilingaryan, *Kvant. Elek.* **9**, 2481–2490 (1982) [*Sov. J. Q. E.* **12**, 1619–25 (1982)].
7. S. D. Durbin, S. M. Arakelian, and Y. R. Shen, *Opt. Lett.* **7**, 145–47 (1982).
8. H. L. Ong, *Phys. Rev.* **A28**, 2392–2407 (1983).
9. H. L. Ong and C. Y. Young, *Phys. Rev.* **A29**, 297–307 (1984).
10. A. Saupe, Private Communciation.
11. R. A. Fisher, *Optical Phase Conjugation* (Academic, 1983).
12. I. C. Khoo and S. L. Zauang, *IEEE J. Q. E.* QE 18, 246–49 (1982).
13. I. C. Khoo and S. Shepard, *J. Appl. Phys.* **54**, 5491–5493 (1983).
14. I. C. Khoo and R. Normandin, *J. Appl. Phys.* **55**, 1416–1418 (1984).
15. I. C. Khoo and R. Normandin *Opt. Lett.* **9**, 285–286 (1984).
16. G. Martin and R. N. Hellwarth, *App. Phys. Lett.* **34**, 371–373 (1979).
17. M. H. Garret and H. J. Hoffman, *J. Opt. Soc. Am.* **73**, 617–623 (1983).
18. P. G. deGennes, *The Physics of Liquid Crystals*, (Clarendon, 1974).
19. D. Armitage, *Applied Optics* (in press).
20. E. Wiener-Avnear, *App. Phys. Lett.* **29**, 635 (1976).
21. H. J. Hoffman and P. E. Perkins, CLEO (1983).
22. H. J. Hoffman, IEEE J. Q. E. (in press).
23. W. H. De Jeu, *Physical Properties of Liquid Crystalline Materials* (Gordon and Breach, 1980).
24. R. G. Horn, *J. De Phy* **39**, 167–172 (1978).
25. H. A. Tarry, RSRE Baldock, unpublished data.
26. M. Brunet-Germain, *C. R. Acad. SC.* **B271**, 1075–1077 (1970).
27. D. Armitage and F. P. Price, *Phys. Rev.* **A15**, 2496–2500 (1977).
28. T. Shinoda, Y. Maeda, and H. Endkido, *J. Chem. Them.* **6**, 921 (1974).
29. D. Armitage, *J. Appl. Phys.* **52**, 1294–1300 (1981).
30. M. Schadt, *J. Chem. Phys.* **71**, 2336–2334 (1979).
31. S. Candau and S. V. Letcher, *Advances in Liquid Crystals*, G. H. Brown, ed. (Academic, 1978).
32. S. Nakai, P. Martinoty, and S. Candau, *J. De Phys.* **37**, 769–780 (1976).
33. F. Rondelez, W. Urbach, and H. Hervert, *Phys. Rev. Lett.* **61**, 1058–1061 (1978).
34. G. Eyring and M. D. Fayer, *J. Chem. Phys.* (in press).